ACS OMEGA

http://pubs.acs.org/journal/acsodf

Article

ROS-Scavenging Selenofluoxetine Derivatives Inhibit *In Vivo* Serotonin Reuptake

Giovanni Ribaudo,[▽] Marco Bortoli,[▽] Colby E. Witt,[▽] Brenna Parke, Sergio Mena, Erika Oselladore, Giuseppe Zagotto, Parastoo Hashemi,* and Laura Orian*

Cite This: *ACS Omega* 2022, 7, 8314–8322

Read Online

ACCESS | Metrics & More | Article Recommendations | Supporting Information

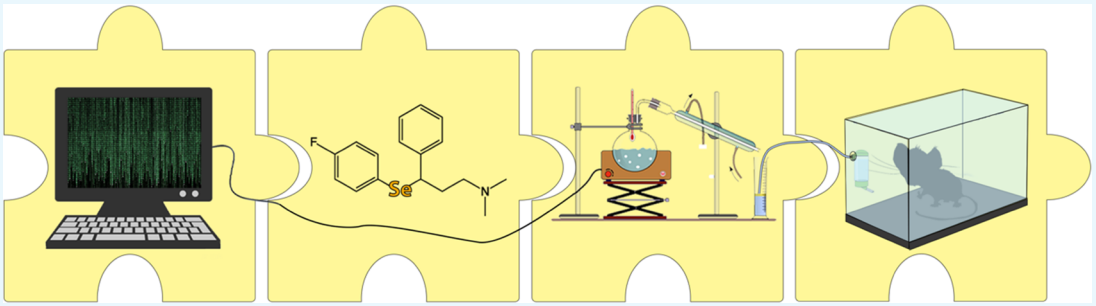

ABSTRACT: While the neurochemistry that underpins the behavioral phenotypes of depression is the subject of many studies, oxidative stress caused by the inflammation comorbid with depression has not adequately been addressed. In this study, we described novel antidepressant−antioxidant agents consisting of selenium-modified fluoxetine derivatives to simultaneously target serotonin reuptake (antidepressant action) and oxidative stress. Excitingly, we show that one of these agents (**1-F**) carries the ability to inhibit serotonin reuptake *in vivo* in mice. We therefore present a frontier dual strategy that paves the way for the future of antidepressant therapies.

INTRODUCTION

The most common therapy for pharmacological treatment of depression are the selective serotonin reuptake inhibitors (SSRIs), which aim to increase serotonin levels in the brain since deficiency of this neuromodulator is thought to underlie depressive-like symptoms in patients. There is now a growing body of evidence that inflammation plays an important role in treatment-resistant depression.[1−4] Inflammation is a blanket term to describe a state of immune activation where immune cells prompt a biochemical cascade (*e.g.*, cytokines) to identify and remove the source of this condition.[5] An important but largely damaging aspect of inflammation is oxidative stress, which is hallmarked by the generation of reactive oxygen species (ROS), nitric oxide (NO), and unbalanced catalase activity.[1,6,7] There are conflicting reports of how SSRIs mediate oxidative stress. It has been reported that venlafaxine (a selective serotonin norepinephrine reuptake inhibitor) and fluoxetine (an SSRI) have direct antioxidant properties.[8−10] Other reports show that fluoxetine can cause hepatotoxicity, and the oxidative stress associated with this toxicity likely offsets any direct antioxidant properties.[11] A clinical study showed that oxidative stress increased in patients successfully treated with antidepressants, including SSRIs.[1] Given that the damaging effects of oxidative stress can be easily curtailed *via* antioxidant therapies that scavenge ROS, there may be important therapeutic potential in combining SSRI and antioxidant therapy.[12]

The Orian group has recently developed a novel antidepressant−antioxidant agent in a selenium-modified fluoxetine molecule.[13] Such druglike chimeric compound is designed with the aim of combining the SSRI effect of fluoxetine with the enhanced antioxidant, ROS-scavenging activity granted by selenium. The substitution of the oxygen atom with the more electropositive chalcogen contributes to scavenging activity, but this activity is strictly related to molecular topology, as recently reported for phenothiazines in which the replacement of sulfur by its heavier siblings does not improve antioxidant potential *per se*.[14] In this work, we describe the synthesis, characterization, and evaluation of two novel selenofluoxetine derivatives and importantly show that the compound named **1-F** maintains the ability to inhibit *in vivo* serotonin reuptake in mice. We therefore present an

Received: October 6, 2021
Accepted: December 31, 2021
Published: March 2, 2022

https://doi.org/10.1021/acsomega.1c05567
ACS Omega 2022, 7, 8314–8322

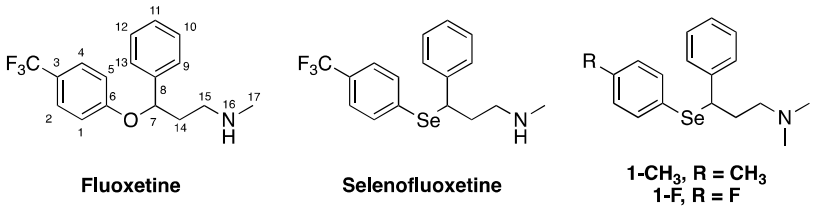

Figure 1. Chemical structure of fluoxetine, selenofluoxetine, and its derivatives studied in this work.

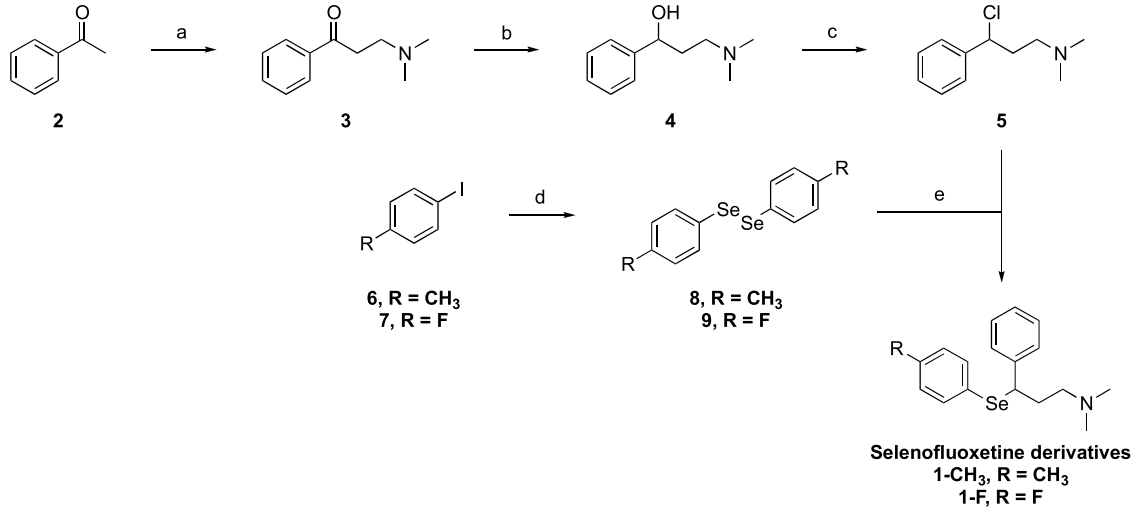

Figure 2. Synthetic scheme for the preparation of selenofluoxetine derivatives: (a) dimethylamine HCl/HCOH/EtOH, 98%; (b) $NaBH_4$/KOH/MeOH, 95%; (c) $SOCl_2$, 96%; (d) Mg/Et_2O, Se, 58% for **8**, 48% for **9**; (e) $NaBH_4$/KOH/EtOH, 49% for **1-CH$_3$**, 47% for **1-F**.

exciting new strategy to target both serotonin and oxidative stress as a next-generation antidepressant.

RESULTS AND DISCUSSION

Bioinspired Modification of Fluoxetine to Create Se Derivatives. Antioxidant potential has been reported for different classes of psychotropic drugs,[12] and fluoxetine itself was previously demonstrated to possess multimechanism antioxidant effects. More precisely, fluoxetine and its metabolites have been described as ROS scavengers and stimulants of the enzymatic and nonenzymatic components of the endogenous antioxidant defense system.[9,10] Potentially offsetting these effects is the hepatotoxicity of fluoxetine that itself creates oxidative stress.[11] We now report novel Se-based derivatives in this paper that are endowed with additional antioxidant potential, a feature that is especially characteristic of organic selenides in the CNS.[15] Serotonin itself is a strong ROS scavenger; thus, we rationalize that the combined antioxidant approach of the Se-based compounds and their effects on increasing extracellular serotonin may work in synergy to strengthen overall antioxidant capability. In fact, computational and *in vitro* experimental evidence demonstrated the antioxidant and radical scavenging properties of serotonin, which play a primary role. Moreover, the influence of fluoxetine metabolites cannot be ruled out.[6,9,10]

The chemical structures of fluoxetine, selenofluoxetine, and its synthesized derivatives investigated in this work are reported in Figure 1.

The preparation of selenofluoxetine derivatives was performed following a convergent synthetic scheme, which was designed based on the approach that we reported previously.[13] Nevertheless, the compounds considered in the current study belong to the class of selenofluoxetines that we presented in a previous paper but show a *p*-CH_3 group and a *p*-F group, which were not described previously. **1-CH$_3$** and **1-F** bear two substituents endowed with openly different electronic and steric features, which allowed us to further explore the role of the modification of the phenyl ring of selenofluoxetine.[13] Thus, the compounds were selected as a representative from this class to carry our investigation to a further level. Both *p*-CH_3 and *p*-F modifications are tolerated modifications according to fluoxetine structure−activity relationship (SAR) studies.[16] Moreover, both compounds, in analogy to fluoxetine, are predicted by SwissADME software to cross the blood−brain barrier.[17] To the extent of synthesizing these derivatives, some modifications were adopted to introduce the *p*-CH_3 and the *p*-F substituents in the final compounds. The overall multistep synthetic scheme for the preparation of **1-CH$_3$** and **1-F** is resumed in Figure 2. Briefly, acetophenone was initially subjected to a *Mannich* reaction giving compound **3**, which was reduced to provide **4** and then chlorinated to obtain the intermediate **5**.[18−20] On the other hand, opportune diselenides **8** and **9** were synthesized by preparing the *Grignard* reagent from the corresponding iododerivatives **6** and **7**, which were then reacted with elemental selenium.[21] The final step of this convergent synthetic scheme consisted in the reaction of intermediate **5** with the selenide nucleophile prepared *in situ* by reduction of **8** or **9**, providing **1-CH$_3$** and **1-F** as the hydrochloride salts. The products were fully characterized by ^{1}H-NMR, ^{13}C-NMR, and ESI-MS (see the Supporting Information for spectra).

In the studied selenofluoxetine derivatives, the oxygen which was originally present in the fluoxetine molecule was replaced by a selenium atom. The choice of the chalcogen is based on

https://doi.org/10.1021/acsomega.1c05567
ACS Omega 2022, 7, 8314−8322

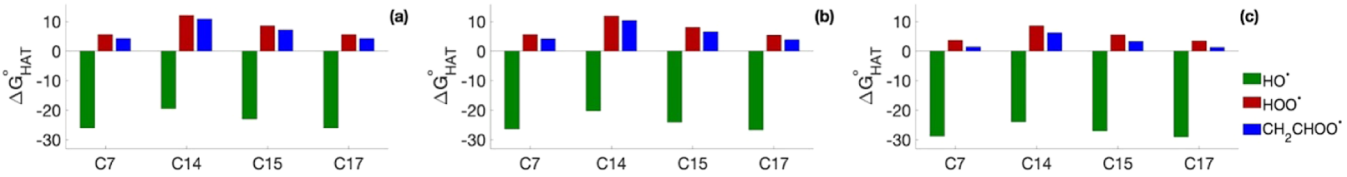

Figure 3. ΔG°_{HAT} (in kcal mol^{-1}) for **1-F** in the gas phase (a), in benzene (b), and in water (c). Level of theory (SMD)-M06-2X/6-311+G(d,p)//M06-2X/6-31G(d,p).

the well-known antioxidant role selenium plays in biology, as a constituent of the catalytic residue of enzymes like glutathione peroxidase (GPx)[22] and thioredoxin reductase (TrxR).[23] Importantly, the synthesis of organoselenides as GPx mimics is still considered an active research task and is worldwide pursued by an active community.[24−31]

Compared to fluoxetine, **1-CH$_3$** and **1-F** bear an *N*,*N*-dimethyl group that was introduced to simplify the synthetic procedures. This modification was previously demonstrated to be tolerated in SAR studies on ligands targeting SERT.[32] Overall, selenofluoxetine derivatives show a close structural similarity with fluoxetine, and thus similar pharmacokinetic and pharmacodynamic properties were expected. Moreover, in analogy with the original compound that inspired this study, the new derivatives were synthesized as hydrochloride salts. In fact, as precisely described by Wong et al. in their review, fluoxetine hydrochloride was originally identified as the ideal form to overcome the limitations of the former oxalate salt in terms of water solubility during the drug development process.[33] Additionally, recent SAR studies based on computational and mechanistic evidence showed that substitutions in the *para* position of fluoxetine with halogen atoms support the activity of such molecules on SERT.[34] On the other hand, derivatives bearing alkyl groups in the *para* position have been investigated as antibacterial agents.[35] Thus, based on the evidence from previous findings, **1-F** was carried to the further level of investigation.

In Silico Modeling of ROS-Scavenging Antioxidant Capacity of Derivatives. Radical scavenging toward three radicals (HO$^{\bullet}$, HOO$^{\bullet}$, and CH$_2$=CHOO$^{\bullet}$) was investigated *in silico* considering hydrogen atom transfer processes (HAT) for **1-F**. *In silico* modeling of the HAT process involves the calculation of the Gibbs free energy of reaction of the abstraction of a H radical by the selected free radical from each suitable site of the ROS scavenger, which results in the formation of the radical form of the selenofluoxetine derivative and the quenched free radical (H$_2$O, H$_2$O$_2$, or CH$_2$=CHOOH). In this work, we focused on the nonaromatic C atoms of the selenofluoxetine derivatives as the most suitable sites for HAT. Results are in agreement with those found for selenofluoxetine[13] and show how sites C7 and C17 are the most favorable for gas-phase HAT reactions (Figure 3). Gibbs free reaction energies are computed to be negative for processes involving HO$^{\bullet}$, whereas in the case of the other radicals, they are found to be positive (Figure 3a).

In the condensed phase, the polarity of the solvent has a common effect on all of the sites, making the reactions progressively more favorable in benzene and water (Figure 3b,c). However, C7 and C17 remain the sites with the lowest (negative) ΔG°_{HAT}, and the trends found in the gas phase are maintained.

This behavior can be qualitatively rationalized by inspecting how the unpaired electron density is distributed on the radical molecule. For example, taking C17 and C14 as a comparison, it is clear how the spin density is more delocalized on the former where it involves the N atom close to C17 compared to C14 where the contribution of adjacent atoms is marginal (Figure 4).

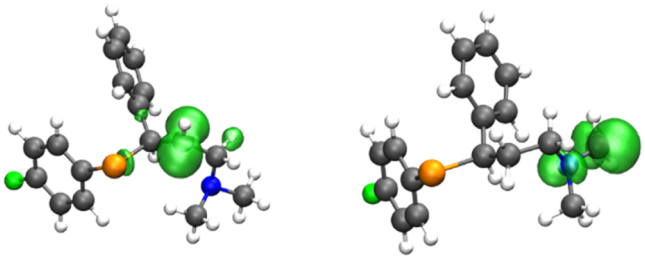

Figure 4. Spin density of two radicals of **1-F** (isosurface value 0.005 a.u.). Level of theory M06-2X/6-311+G(d,p)//M06-2X/6-31G(d,p).

To gain a deeper insight into the kinetics of the HAT processes, the reaction with HO$^{\bullet}$ was furtherly investigated to obtain the activation energies in the gas phase and in solution. Results show that the computed activation energies are very low and that the sites for which HATs are most exergonic, namely, C7 and C17, are also the two that display the lowest reaction barriers, confirming once again the agreement with the Bell−Evans−Polanyi principle, which states that the reaction with the lowest activation barriers is also the most thermodynamically favored, and supporting the idea of a simplification of the analysis of HAT processes proposed in previous works (Table 1).[6,7,36,37]

Table 1. Activation Free Energies (kcal mol^{-1}) for HAT Reactions Involving 1-F and HO$^{\bullet}$. Level of Theory (SMD)-M06-2X/6-311+G(d,p)//M06-2X/6-31G(d)

site	gas phase[a]	benzene[a]	water[a]
C7	2.3	3.6	3.3
C14	8.4	10.0	9.6
C15	5.6	6.5	5.0
C17	5.5	5.9	2.5

1-F inhibits In Vivo Serotonin Reuptake in Mice. A deficit in extracellular brain serotonin has long been thought to underlie the pathology of depression, as such SSRIs are the frontline clinical treatment for the disorder. SSRIs are small organic molecules, structurally resembling serotonin, that inhibit the serotonin transporter (SERT), a protein tasked with clearing the monoamine after synaptic release. However, the therapeutic mechanism of action of SSRIs remains unknown since the effects of these drugs on *in vivo* serotonin chemistry in the brain are hard to assess. Over the past decade, Hashemi and colleagues have developed a niche tool for monitoring *in vivo* serotonin in rodent models using

https://doi.org/10.1021/acsomega.1c05567
ACS Omega 2022, 7, 8314−8322

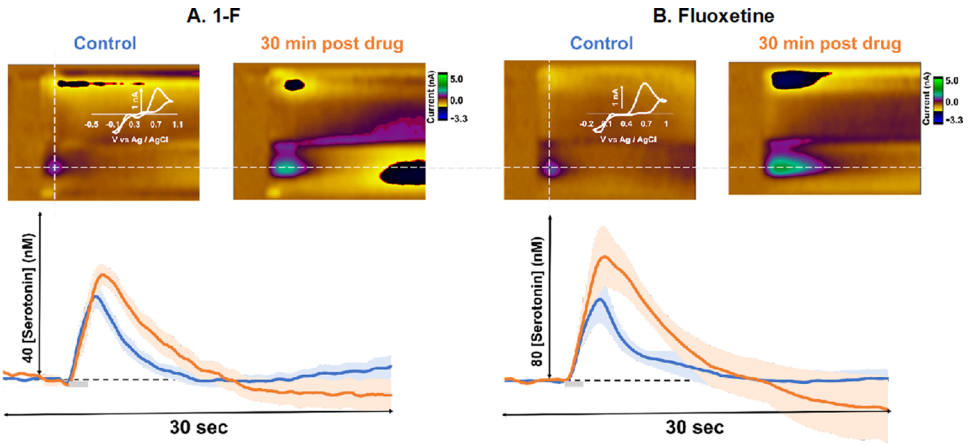

Figure 5. *In vivo* stimulated serotonin release in the CA2 region of the hippocampus. (A) Representative color plots for this experimental paradigm, before and 30 min into drug analysis, are found above the representative IT curves. The averaged control evoked serotonin in mixed-sex cohort can be found in blue (n = 5) with SEM calculated and outlined in the lighter shade of blue. The averaged drug files (**1-F**, 50 mg kg^{-1}) at 30 min for serotonin in mixed-sex cohort is plotted in orange (n = 5) with SEM calculated and outlined in the lighter shade of orange. Stimulation is indicated by the gray bar. (B) Representative color plots for this experimental paradigm, before and 30 min into drug analysis, are found above the representative IT curves. The averaged control evoked serotonin in mixed-sex cohort can be found in blue (n = 5) with SEM calculated and outlined in the lighter shade of blue. The averaged drug files (Fluoxetine, 20 mg kg^{-1}) at 30 min for serotonin in mixed-sex cohort is plotted in orange (n = 5) with SEM calculated and outlined in the lighter shade of orange. Stimulation is indicated via the gray bar. Statistical analysis can be found for each data set in Table 2.

FSCV.[38−42] Briefly, FSCV involves implantation of a CFM directly into the brain of an anesthetized mouse and applying an electrochemical waveform; direct electrochemical redox of the molecules enables identification and quantification of serotonin in real time, with subsecond time resolution.[39,43] This method was used in a series of studies to evaluate the effects of escitalopram, a common SSRI, on electrically evoked serotonin in the CA2 region of the hippocampus in mice. Escitalopram rapidly and profoundly increased release amplitude and decreased reuptake rate of serotonin.[38,41]

In this work, we asked whether the novel selenofluoxetine derivatives were capable of inhibiting *in vivo* serotonin reuptake in a similar manner to the previous escitalopram studies. A control serotonin signal was isolated in five mice in the CA2 region of the hippocampus in a mixed-sex cohort (Figure 5A: blue). After four control files were collected, **1-F** was administered *via i.p.* injection at 50 mg kg^{-1} in saline (readily soluble). Saline alone does not affect ambient serotonin dynamics.[44] After 30 min, the signal was taken and averaged between the mice (Figure 5A orange), this time was chosen as it was the point of maximal response and is in line with the half-life of other common SSRIs in mice.[45] Serotonin release amplitude increased from 22.73 ± 4.07 to 25.84 ± 3.41 nM (N.S.), and the $t_{1/2}$ of reuptake was found to significantly increase from 1.93 ± 0.30 to 3.38 ± 0.41 s (p < 0.05). A further set of experiments, in a separate mouse cohort, was performed in the same way with the analogous model fluoxetine at 20 mg kg^{-1} (Figure 5B: orange). We found a significant amplitude increase from 35.75 ± 10.16 to 56.05 ± 13.40 nM and a significant $t_{1/2}$ increase from 1.90 ± 0.46 to 4.01 ± 0.70 s (p < 0.05).

Fluoxetine has a more pronounced effect on the serotonin signal than **1-F**, despite the lower dose. We believe this is a consequence of two effects. First, the electronegativity conferred by the oxygen group in fluoxetine plays an important role in the way the SSRI binds to the SERTs.[42] Second, the Se−C bond could be more easily hydrolyzed than the O−C bond because the valence electrons in the Se−C bond are more shielded from the nucleus given the Se atom.[39] Nevertheless, preliminary HPLC analysis carried out at different time points on the studied compounds highlighted that the molecules are stable in aqueous solution for a time that is longer than that considered in the *in vivo* experiments (HPLC chromatograms are reported in the Supporting Information). On the other hand, this new agent does have the ability to inhibit serotonin reuptake, and therefore this opens a path for an additional approach against depression. Further evidence to support the effects on serotonin reuptake of this newly developed compound is our Michaelis−Menten analysis. For both fluoxetine and the new analogue, we see that V_{max} (maximum rate of reuptake) decreases upon the administration of the agent. For fluoxetine, V_{max} trends from 17.69 to 15.21 nM/s, and for **1-F**, it trends from 15.60 to 13.46 nM/s. Thus, our new compounds show promising chemical efficacy for slowing serotonin reuptake (Table 2).

Table 2. Features of In Vivo Experimental Curves: Mean ± SEM (n = 5 animals) of the Maximum Evoked Serotonin Amplitude (*Ampmax*) and Clearance Rate ($t_{1/2}$)[a]

	maximum release (nM)	$t_{1/2}$ of clearance (s)	V_{max} (nM/s)
control pre-fluoxetine	35.75 ± 10.16	1.90 ± 0.46	17.69
30 min post-fluoxetine	56.05 ± 13.40*	4.01 ± 0.70*	15.21
control pre-1-F	22.73 ± 4.07	1.93 ± 0.30	15.60
30 min post-1-F	25.84 ± 3.41	3.38 ± 0.41*	13.46

[a]Each parameter was tested for significant difference between control and drug treatment (paired samples t-test). Significance (*) was defined as p < 0.05. Michaelis−Menten reuptake kinetics model for serotonin was fitted to the signal. K_m was set to 5 nM, while V_{max} was optimized to fit the average experimental trace.

https://doi.org/10.1021/acsomega.1c05567
ACS Omega 2022, 7, 8314−8322

CONCLUSIONS

Depression and inflammation are highly comorbid and, consequently, there is potential for oxidative stress in depression patients. Besides, there is conflicting information on whether SSRIs have oxidant properties. Therefore, in this work, we described novel agents to simultaneously target serotonin uptake and oxidative stress. We synthesized and characterized these new selenofluoxetine derivatives and importantly showed that **1-F** carries the ability to inhibit serotonin reuptake. Thus, we presented an exciting dual strategy that paves the way for future antidepressant therapies.

MATERIALS AND METHODS

Chemistry. Commercially available chemicals were purchased from Sigma-Aldrich and used without any further purification. NMR experiments were performed on a Bruker Avance III 400 spectrometer (frequencies: 400.13 and 100.62 MHz for ^{1}H and ^{13}C, respectively) (Bruker, Billerica, MA) equipped with a multinuclear inverse z-field gradient probe head (5 mm). For data processing, TopSpin 4.0.8 software was used, and the spectra were calibrated using solvent signal (^{1}H-NMR, δ_H = 7.26 ppm for $CDCl_3$, δ_H = 2.50 ppm for DMSO-d_6, δ_H = 4.79 ppm for D_2O; ^{13}C-NMR, δ_C = 77.16 ppm for $CDCl_3$, δ_C = 39.52 ppm for DMSO). Mass spectra were recorded by direct infusion electrospray (ESI) on an LCQ Fleet ion trap mass spectrometer (Thermo Fisher Scientific, Waltham, MA) and on a Xevo G2 QTof high-resolution mass spectrometer (HRMS; Waters, Milford, MA). ^{1}H-NMR, ^{13}C-NMR, and ESI-MS spectra are reported in the Supporting Information. The purity profile was assayed by HPLC using a Pro-Star system (Palo Alto, CA) equipped with a 1706 UV−VIS detector (Bio-Rad, Hercules, CA) and a C-18 column (5 μm, 4.6 × 150 mm) (Agilent, Santa Clara, CA). An appropriate gradient of 0.1% formic acid (A) and acetonitrile (B) was used as mobile phase with an overall flow rate of 1 mL min^{-1}. The general method for the analyses is reported in the following: 0 min (60% A−40% B), 5 min (90% A−10% B), 6 min (90% A−10% B), 8 min (60% A−40% B), and 32 min (90% A−10% B). Analyses were performed at 254 nm.

*Synthesis of N,N-Dimethyl-3-oxo-3-phenylpropan-1-aminium chloride (**3**).* Dimethylamine hydrochloride (2.03 g, 24.9 mmol, 1.5 equiv) and paraformaldehyde (0.65 g, 21.6 mmol, 1.3 equiv) were introduced in a 50 mL round-bottom flask and dissolved in 2.5 mL of ethanol. Acetophenone (2.00 g, 16.6 mmol, 1 equiv) was added to the solution together with 40 μL of concentrated HCl. The reaction mixture was stirred at reflux and monitored by TLC (DCM/MeOH/TEA 97:2.5:0.5). After 2 h, the solution was cooled to room temperature. A solid precipitate of *N,N*-dimethyl-3-oxo-3-phenylpropan-1-aminium chloride salt formed. The solid was filtered using a Buchner funnel and washed with cold acetone (3 × 10 mL) and hexane (1 × 10 mL). Yield 3.48 g (98%); white solid; ^{1}H-NMR (400 MHz, DMSO): δ_H (ppm) 10.57 (br, 1H, N*H*), 8.02 (d, 2H, *J* = 7.2 Hz, Ph-*H*), 7.69 (t, 1H, *J* = 7.4 Hz, Ph-*H*), 7.57 (t, 2H, *J* = 7.6 Hz, Ph-*H*), 3.63 (t, 2H, *J* = 7.2 Hz, C(O)C*H*$_2$), 3.40 (t, 2H, *J* = 7.2 Hz, C*H*$_2$N), 2.80 (s, 6H, N(C*H*$_3$)$_2$); ^{13}C-NMR (101 MHz, DMSO): δ_C (ppm) 196.8 (s, C(O)), 135.9 (s, Ph-*C*), 133.7 (s, 2C, Ph-*C*), 128.8 (s, Ph-*C*), 128.0 (s, 2C, Ph-*C*), 51.8 (s, *C*H$_2$N), 42.2 (s, 2C, N(*C*H$_3$)$_2$), 33.1 (s, C(O)*C*H$_2$); (ESI+) *m*/*z* calcd for $C_{11}H_{16}NO^+$ [M + H]$^+$: 178.1232; found: 178.1308.

*Synthesis of 3-Hydroxy-N,N-dimethyl-3-phenylpropan-1-amine (**4**).* Compound **3** (1.80 g, 8.39 mmol, 1 equiv) was dissolved in 5 mL of distilled water, and 1.2 mL of 8 M KOH was added to the mixture. A white solid formed, and the mixture was extracted with DCM (4 × 20 mL). The organic phases were combined, and the solvent was evaporated under reduced pressure, yielding the free base of compound **3**. The oily residue was dissolved in 10 mL of methanol, and a couple of drops of 8 M KOH were added. The solution was cooled to 0 °C, and $NaBH_4$ (0.47 g, 12.6 mmol, 3 equiv) was added to the solution. After the dissolution of all of the reactants, the ice bath was removed and the mixture was stirred at room temperature for 1.5 h. Concentrated HCl was added dropwise until acid pH, and the solution was then basified with KOH 8 M. Methanol was evaporated under reduced pressure, and the resulting solid was dissolved in 100 mL of DCM and washed with alkaline water (4 × 10 mL). The organic phase was dried with anhydrous $MgSO_4$, filtered, and evaporated under reduced pressure. Yield 1.43 g (95%); colorless oil; ^{1}H-NMR (400 MHz, $CDCl_3$): δ_H (ppm) 7.41−7.31 (m, 4H, Ph-*H*), 7.28−7.22 (m, 1H, Ph-*H*), 4.91 (dd, *J* = 7.1, 4.7 Hz, 1H, C*H*(OH)), 2.66−2.58 (m, 1H, CH(OH)C*H*$_A$H$_B$), 2.48−2.42 (m, 1H, CH(OH)CH$_A$*H*$_B$), 2.28 (s, 6H, N(C*H*$_3$)$_2$), δ_H 1.86−1.79 (m, 2H, C*H*$_2$N); ^{13}C-NMR (101 MHz, $CDCl_3$): δ_C (ppm) 145.1 (s, Ph-*C*), 128.1 (s, 2C, Ph-*C*), 126.8 (s, Ph-*C*), 125.5 (s, 2C, Ph-*C*), 75.3 (s, *C*H(OH)), 58.1 (s, *C*H$_2$N), 45.2 (s, 2C, N(*C*H$_3$)$_2$), 34.7 (s, CH(OH)*C*H$_2$); (ESI+) *m*/*z* calcd for $C_{11}H_{18}NO^+$ [M + H]$^+$: 180.14, found: 180.11.

*Synthesis of 3-Chloro-N,N-dimethyl-3-phenylpropan-1-aminium chloride (**5**).* Compound **4** (1.50 g, 8.37 mmol) was dissolved in a small amount of diethyl ether, and 5 mL of 2 M HCl in ether was added to obtain the corresponding hydrochloride salt. The solvent was evaporated under reduced pressure and 10 mL of thionyl chloride was subsequently added to the round-bottom flask. The resulting solution was stirred under reflux, and the reaction was monitored by TLC (DCM/MeOH/TEA 97:2.5:0.5). After 2 h, the solvent was evaporated under reduced pressure obtaining the compound as a hydrochloride salt. Yield 1.88 g (96%), white solid; ^{1}H-NMR (400 MHz, DMSO): δ_H (ppm) 10.90 (br, 1H, N*H*), 7.52−7.49 (m, 2H, Ph-*H*), 7.45−7.35 (m, 3H, Ph-*H*), 5.31 (dd, *J* = 9.1, 5.2 Hz, 1H, C*H*(Cl)), 3.23−3.18 (m, 1H, CH(Cl)-C*H*$_A$H$_B$), 3.10−3.04 (m, 1H, CH(Cl)CH$_A$*H*$_B$), 2.76 (s, 6H, N(C*H*$_3$)$_2$), 2.63−2.44 (m, 2H, C*H*$_2$N); ^{13}C-NMR (101 MHz, DMSO): δ_C (ppm) 141.0 (s, Ph-*C*), 129.3 (s, 2C, Ph-*C*), 129.2 (s, 2C, Ph-*C*), 127.5 (s, Ph-*C*), 61.1 (s, *C*H(Cl)), 42.7 (s, *C*H$_2$N), 42.4 (s, 2C, N(*C*H$_3$)$_2$), 33.6 (s, CH(Cl)*C*H$_2$); (ESI+) *m*/*z* calcd for $C_{11}H_{17}ClN^+$ [M + H]$^+$: 198.10, found: 198.10.

*Synthesis of 1,2-Di-p-tolyldiselane (**8**).* Under nitrogen atmosphere, magnesium chips (78 mg, 3.21 mmol, 1 equiv) were introduced in a 50 mL three-neck round-bottom flask. A solution of *p*-iodotoluene (700 mg, 3.21 mmol 1 equiv) in 10 mL of dry ether was added dropwise at gentle reflux, and the mixture was stirred for another 30 min. Afterward, selenium powder (254 mg, 3.21 mmol, 1 equiv) was added under gentle reflux and the reaction mixture was stirred for another 30 min. The reaction was then poured into a mixture of cracked ice and concentrated HCl. The cold mixture was extracted with ether (3 × 20 mL). The combined organic layers were dried using $MgSO_4$ and filtered. The solvent was removed under reduced pressure giving the product. Yield 316 mg (58%); orange oil; ^{1}H-NMR (400 MHz, $CDCl_3$): δ_H (ppm) 7.56 (d, *J* = 8.09 Hz, 4H, Ph-*H*), 7.12 (d, *J* = 8.09 Hz, 4H, Ph-*H*), 2.39 (s, 6H, Ph-

https://doi.org/10.1021/acsomega.1c05567
ACS Omega 2022, 7, 8314−8322

CH_3); ^{13}C-NMR (101 MHz, $CDCl_3$): δ_C (ppm) 138.0 (s, Ph-*C*), 132.4 (s, Ph-*C*), 130.0 (s, Ph-*C*), 126.9 (s, Ph-*C*), 21.2 (s, Ph-CH_3).

*Synthesis of 1,2-Bis(4-fluorophenyl)diselane (**9**).* Under nitrogen atmosphere, magnesium chips (97 mg, 4 mmol, 1 equiv) were introduced in a 50 mL three-neck round-bottom flask. A solution of 1-fluoro-4-iodobenzene (700 mg, 4 mmol 1 equiv) in 10 mL of dry ether was added dropwise at gentle reflux, and the mixture was stirred for another 30 min. Afterward, selenium powder (316 mg, 4 mmol, 1 equiv) was added maintaining gentle refluxing and the reaction mixture was stirred for another 30 min. The reaction was then poured in a mixture of cracked ice and concentrated HCl. The cold mixture was extracted with ether (3 × 20 mL). The combined organic layers were dried using $MgSO_4$ and filtered. The solvent was removed under reduced pressure giving the product. Yield 331 mg (48%); ^{1}H-NMR (400 MHz, DMSO): δ_H (ppm) 7.68−7.63 (m, 4H, Ph-*H*), 7.24−7.18 (m, 4H, Ph-*H*).

*Synthesis of N,N-Dimethyl-3-phenyl-3-(p-tolylselanyl)-propan-1-amine (**1-CH$_3$**).* Compound **8** (316 mg, 0.93 mmol, 1 equiv) was introduced in a 50 mL round-bottom flask and dissolved in ethanol (10 mL). KOH (157 mg, 2.79 mmol, 3 equiv) was added, and the solution was cooled in an ice bath, followed by the addition of $NaBH_4$ (211 mg, 5.58 mmol, 6 equiv). After 1 h, once the mixture changed its color, compound **5** (218 mg, 0.93 mmol, 1 equiv) was added to the solution. The reaction was stirred at room temperature for 3 h. To quench the unreacted $NaBH_4$, concentrated HCl was added to the mixture until acid pH. Afterward, 8 M KOH was added until basic pH. Ethanol was evaporated under reduced pressure, and the resulting solid was dissolved in DCM (30 mL). The solution was washed with alkaline water (3 × 15 mL), dried over magnesium sulfate, and filtered. The solvent was evaporated under reduced pressure, and the crude product was purified by column chromatography (silica gel, DCM:MeOH:TEA 92:7.5:0.5). Yield: 152 mg (49%); yellow solid; HPLC: 96% (percentage area, 254 nm); ^{1}H-NMR (400 MHz, $CDCl_3$): δ_H (ppm) 7.30−7.18 (m, 7H, Ph-*H*), 7.03 (d, *J* = 7.9 Hz, 2H, Ph-*H*), 4.30−4.27 (m, 1H, C*H*(Se)), 2.33 (s, 3H Ph-CH_3), 2.32−2.20 (m, 4H, CH-CH_2-CH_2-N), 2.18 (s, 6H, $N(CH_3)_2$); ^{13}C-NMR (101 MHz, $CDCl_3$): δ_C (ppm) 142.6 (s, Ph-*C*), 138.0 (s, Ph-*C*), 136.0 (s, Ph-*C*), 129.7 (s, Ph-*C*), 128.4 (s, Ph-*C*), 127.8 (s, Ph-*C*), 126.9 (s, Ph-*C*), 125.7 (s, Ph-*C*), 58.1 (s, *C*H(Se)), 46.2 (s, CH_2N), 45.6 (s, $N(CH_3)_2$), 33.9 (s, CH(Se)CH_2), 21.3 (Ph-CH_3); (ESI+) *m*/*z* calcd for $C_{18}H_{24}NSe^+$ $[M + H]^+$: 334.1068, found 334.1112.

*Synthesis of 3-((4-Fluorophenyl)selanyl)-N,N-dimethyl-3-phenylpropan-1-amine (**1-F**).* Compound **9** (331 mg, 0.95 mmol, 1 equiv) was introduced in a 50 mL round-bottom flask and dissolved in ethanol (10 mL). KOH (160 mg, 2.85 mmol, 3 equiv) was added and the solution was cooled in an ice bath, followed by the addition of $NaBH_4$ (216 mg, 5.70 mmol, 6 equiv). After 1 h, once the mixture changed its color, compound **5** (223 mg, 0.95 mmol, 1 equiv) was added to the solution. The reaction was stirred at room temperature for 3 h. To quench the unreacted $NaBH_4$, concentrated HCl was added to the mixture until acid pH. Afterward, 8 M KOH was added until basic pH. Ethanol was evaporated under reduced pressure, and the resulting residue was dissolved in DCM (30 mL). The solution was washed with alkaline water (3 × 15 mL), dried over magnesium sulfate, and filtered. The solvent was evaporated under reduced pressure, and the product was purified by column chromatography (silica gel, DCM/MeOH/TEA 92:7.5:0.5). Yield: 151 mg (47%); yellow solid; HPLC: 96% (percentage area, 254 nm); ^{1}H-NMR (400 MHz, $CDCl_3$): δ_H (ppm) 7.32−7.28 (m, 2H, Ph-*H*), 7.24−7.15 (m, 3H, Ph-*H*), 7.12−7.10 (m, 2H, Ph-*H*), 6.89−6.84 (m, 2H, Ph-*H*), 4.27−4.23 (m, 1H, C*H*(Se)), 2.37−2.13 (m, 4H, Se-CH_2CH_2), 2.19 (s, 6H, $N(CH_3)_2$); ^{13}C NMR (101 MHz, $CDCl_3$) δ_C (ppm) 164.3 (Ph-*C*), 138.3 (Ph-*C*), 138.2 (Ph-*C*), 128.5 (Ph-*C*), 127.8 (Ph-*C*), 127.1 (Ph-*C*), 116.1 (Ph-*C*), 115.9 (Ph-*C*), 57.9 (s, *C*H(Se)), 46.6 (s, CH_2N), 45.3 (s, $N(CH_3)_2$), 33.4 (s, CH(Se)CH2); (ESI+) calcd for $C_{17}H_{22}FNSe^+$ $[M + H]^+$: 338.0818, found 338.0065.

Computational Methods. For all of the hydrogen atom transfer (HAT) reactions, geometry optimizations of the reactants and products were performed in the gas phase without any constraint, using the M06-2X functional[46] combined with the 6-31G(d) basis set, as implemented in Gaussian 16.[47] Spin contamination was checked for the doublet ground state species to assess the reliability of the wavefunction. Frequency calculations at the M06-2X/6-31G(d) level of theory were run to confirm the nature of the stationary points and to obtain the thermodynamic corrections at 1 atm and 298 K. This procedure ascertained that only positive frequencies were present in minimum-energy structures and a single negative frequency with the correct vibrational mode in transition state structures. To obtain more accurate energy values, single-point energy calculations were performed at M06-2X/6-311+G(d,p) in the gas phase, and subsequently, in benzene and water, at the same level of theory, using the continuum solvation model based on density (SMD).[48] This level of theory is referred to in the text as (SMD)-M06-2X/6-311+G(d,p)//M06-2X/6-31G(d,p). Benzene and water represent an apolar and a polar environment, respectively,[49] and were therefore chosen to adequately investigate the scavenging activity in different environments.

Electrode Fabrication and Animal Work. Carbon Fiber Microelectrodes (CFMs) were made individually by aspirating a single carbon fiber (Goodfellow Corporation, PA) into a 0.6 mm × 0.4 mm glass capillary (A-M Systems, Inc., Sequim, WA). The capillary was then pulled by a vertical puller (Narishige, Tokyo, Japan) to create a seal. The carbon fiber was then trimmed to 150 ± 5 μm for serotonin electrodes. Liquion (LQ-1105, 5% by weight Nafion) (New Castle, DE) was electrodeposited onto the surface of the carbon fiber by dipping and applying a constant potential of +1.0 V for 30 s. The electrode was then dried at 70 °C for 10 min and used after 24 h. The CFM was placed in the CA2 region of the hippocampus of C57BL/6J mice models (Jackson Laboratory, Bar Harbor, ME). These mice were injected with a 25% urethane solution based on a calculation that is dependent on their weight (7 μL/g) in their intraperitoneal cavity (*i.p.*). Following anesthetic administration, the mouse was placed into a stereotaxic system (David Kopf Instruments, Tujunga, CA), where body temperature was maintained *via* a heating pad (Braintree Scientific, Braintree, MA). Three holes were drilled into the skull of the mouse based off coordinates from the mouse brain atlas. The working electrode was placed in the CA2 region of the hippocampus (CA2: −2.91, +3.35, −2.50); the stimulating electrode (insulated stainless steel, diameter 0.2 mm, untwisted, Plastics One, Roanoke, VA) was placed in the medial forebrain bundle (MFB: −1.58, +1.00, −4.80); and the pseudo-AglAgCl reference electrode (made by plating Cl^- onto the surface of an Ag wire) was placed in the opposite

https://doi.org/10.1021/acsomega.1c05567
ACS Omega 2022, 7, 8314−8322

hemisphere of the brain as the working and stimulating electrodes. Stimulation was accomplished via linear constant current stimulus isolator (NL800A Neurolog, Medical Systems Corp, Great Neck, NY) with the following parameters: 60 Hz, 360 μA each, 2 ms in width, and 2 s in length. Animal use followed NIH guidelines and complied with the University of South Carolina Institutional Animal Care and Use Committee under an approved protocol.

FSCV Acquisition and Analysis. FSCV was performed using a Dagan Potentiostat (Dagan Corporation, Minneapolis, MN), National Instruments multifunction device USB-6341 (National Instruments, Austin, TX), WCCV 4.0 software (Knowmad Technologies LLC, Tucson, AZ), and a Pine Research headstage (Pine Research Instrumentation, Durham, NC). The data were filtered (zero phase, Butterworth, 2 kHz low-pass) and smoothed via applications built into the WCCV software. The "Jackson" waveform was applied to elicit the redox properties of serotonin (5-HT: +0.2 V to +1.0 V to −0.1 V to +0.2 V, 1000 V s^{-1}). For FSCV data collection, this was applied at 10 Hz, and cyclic voltammograms were used to confirm that serotonin was elicited as well as current vs time traces were used to visualize the release and reuptake of serotonin. Data presented include four evoked stim files (control) with 10 min between each event averaged and standard error of the mean displayed for error analysis and 30 min after drug administration (fluoxetine or selenofluoxetine) with error again displayed as the standard error of the mean. These files were converted to concentration via a previously determined calibration factor (49.5 ± 10.2 nA/μM). Statistical significance was determined via a two-tailed t-test ($p < 0.05$). All parametric and kinetic analyses were performed using The Analysis Kid.[50] Maximum amplitude of evoked serotonin release and clearance rate of the reuptake curve ($t_{1/2}$) were measured for each individual FSCV acquisition. The maximum amplitude is automatically determined using a custom-designed peak-finding algorithm. An exponential decay curve was fitted to the reuptake of the experimental traces to estimate the half-life of the neurotransmitter release. A previously described Michaelis−Menten model with two reuptake processes[38] was fitted to the average FSCV trace of each treatment group. For each average trace, K_m was kept with a constant value of 5 nM, while V_{max} was optimized to fit the signal using the root-mean-square error between the model and the experimental trace as the cost function.

We utilized previously collected sample data to determine statistical significance between two serotonin signals.[42] Based on Charan and Kantharia,[51] a power analysis was carried out with these data. The following formula was used to calculate the sample size between two groups

$$n = 2\mathrm{SD}^2(Z^\alpha + Z^\beta)/d^2$$

From these sample data, the pooled standard deviation was 1.06, with the effect size being 1.96, which resulted in a Cohen's d of 1.85.[52] Using a 95% confidence interval, Z^α was 1.96 and Z^β was 0.842, assuming 80% power. The power analysis resulted in n = 5.25, which was rounded down to five.

■ ASSOCIATED CONTENT

Supporting Information

The Supporting Information is available free of charge at https://pubs.acs.org/doi/10.1021/acsomega.1c05567.

^{1}H-NMR, ^{13}C-NMR, and ESI-MS characterization spectra of the compounds; HPLC analysis at different time points for compounds **1-F** and **1-CH$_3$**; and coordinates of the in silico optimized structures (PDF)

■ AUTHOR INFORMATION

Corresponding Authors

Laura Orian − *Dipartimento di Scienze Chimiche, Università degli Studi di Padova, 35131 Padova, Italy;* orcid.org/0000-0002-1673-5111; Email: laura.orian@unipd.it

Parastoo Hashemi − *Department of Bioengineering, Imperial College London, London SW7 2AZ, U.K.; Department of Chemistry and Biochemistry, University of South Carolina, Columbia, South Carolina 29201, United States;* orcid.org/0000-0002-0180-767X; Email: p.hashemi04@imperial.ac.uk

Authors

Giovanni Ribaudo − *Dipartimento di Medicina Molecolare e Traslazionale, Università degli Studi di Brescia, 25123 Brescia, Italy;* orcid.org/0000-0003-3679-5530

Marco Bortoli − *Dipartimento di Scienze Chimiche, Università degli Studi di Padova, 35131 Padova, Italy; Institut de Química Computacional i Catàlisi and Departament de Química, Universitat de Girona, 17003 Girona, Catalonia, Spain;* orcid.org/0000-0001-5506-6347

Colby E. Witt − *Department of Chemistry and Biochemistry, University of South Carolina, Columbia, South Carolina 29201, United States;* Present Address: Department of Chemistry at the University of Cincinnati, 312 Clifton Ct, Cincinnati, Ohio 45221, United States

Brenna Parke − *Department of Bioengineering, Imperial College London, London SW7 2AZ, U.K.*

Sergio Mena − *Department of Bioengineering, Imperial College London, London SW7 2AZ, U.K.*

Erika Oselladore − *Dipartimento di Medicina Molecolare e Traslazionale, Università degli Studi di Brescia, 25123 Brescia, Italy*

Giuseppe Zagotto − *Dipartimento di Scienze del Farmaco, Università degli Studi di Padova, 35131 Padova, Italy;* orcid.org/0000-0001-7053-4196

Complete contact information is available at: https://pubs.acs.org/10.1021/acsomega.1c05567

Author Contributions

$^\nabla$G.R., M.B., and C.E.W. contributed equally to this work.

Notes

The authors declare no competing financial interest.

■ ACKNOWLEDGMENTS

This research was funded by the Università degli Studi di Padova, thanks to the P-DiSC (BIRD2018-UNIPD) project MAD^{3}S (Modeling Antioxidant Drugs: Design and Development of computer-aided molecular Systems). Principal investigator: L.O. Calculations were carried out on the system Bastion provided by the CNAF (https://www.cnaf.infn.it/, Bologna Italy), thanks to the ISCRA C project INCIPIT (Insight on Chalcogen Nitrogen Interaction, HP10C15ZCK). Principal investigator: M.B. G.R., and E.O. acknowledge funding from University of Brescia. The Eli Lilly Young Investigator Award for Analytical Chemistry (PH), Imperial

College, and the National Institutes of Health R01MH106563 (PH) supported this work.

REFERENCES

(1) Lindqvist, D.; Dhabhar, F. S.; James, S. J.; Hough, C. M.; Jain, F. A.; Bersani, F. S.; Reus, V. I.; Verhoeven, J. E.; Epel, E. S.; Mahan, L.; Rosser, R.; Wolkowitz, O. M.; Mellon, S. H. Oxidative Stress, Inflammation and Treatment Response in Major Depression. *Psychoneuroendocrinology* **2017**, *76*, 197−205.
(2) Lee, C.-H.; Giuliani, F. The Role of Inflammation in Depression and Fatigue. *Front. Immunol.* **2019**, *10*, No. 1696.
(3) Bajpai, A. Oxidative Stress and Major Depression. *J. Clin. Diagn. Res.* **2014**, *8*, CC04−CC07.
(4) Salim, S. Oxidative Stress and the Central Nervous System. *J. Pharmacol. Exp. Ther.* **2017**, *360*, 201−205.
(5) Ryan, G. B.; Majno, G. Acute Inflammation. A Review. *Am. J. Pathol.* **1977**, *86*, 183−276.
(6) Muraro, C.; Polato, M.; Bortoli, M.; Aiolli, F.; Orian, L. Radical Scavenging Activity of Natural Antioxidants and Drugs: Development of a Combined Machine Learning and Quantum Chemistry Protocol. *J. Chem. Phys.* **2020**, *153*, No. 114117.
(7) Galano, A.; Raúl Alvarez-Idaboy, J. Computational Strategies for Predicting Free Radical Scavengers' Protection against Oxidative Stress: Where Are We and What Might Follow? *Int. J. Quantum. Chem.* **2019**, *119*, No. e25665.
(8) Kumar, A.; Garg, R.; Gaur, V.; Kumar, P. Venlafaxine Involves Nitric Oxide Modulatory Mechanism in Experimental Model of Chronic Behavior Despair in Mice. *Brain Res.* **2010**, *1311*, 73−80.
(9) Caiaffo, V.; Oliveira, B. D. R.; Sá, F. B.; Evêncio Neto, J. Anti-inflammatory, Antiapoptotic, and Antioxidant Activity of Fluoxetine. *Pharmacol. Res. Perspect.* **2016**, *4*, No. e00231.
(10) Kolla, N.; Wei, Z.; Richardson, J. S.; Li, X.-M. Amitriptyline and Fluoxetine Protect PC12 Cells from Cell Death Induced by Hydrogen Peroxide. *J. Psychiatry Neurosci.* **2005**, *30*, 196−201.
(11) Tutakhail, A.; Nazari, Q. A.; Khabil, S.; Gardier, A.; Coudore, F. Muscular and Mitochondrial Effects of Long-Term Fluoxetine Treatment in Mice, Combined with Physical Endurance Exercise on Treadmill. *Life Sci.* **2019**, *232*, No. 116508.
(12) Ribaudo, G.; Bortoli, M.; Pavan, C.; Zagotto, G.; Orian, L. Antioxidant Potential of Psychotropic Drugs: From Clinical Evidence to In Vitro and In Vivo Assessment and toward a New Challenge for in Silico Molecular Design. *Antioxidants* **2020**, *9*, 714.
(13) Ribaudo, G.; Bortoli, M.; Ongaro, A.; Oselladore, E.; Gianoncelli, A.; Zagotto, G.; Orian, L. Fluoxetine Scaffold to Design Tandem Molecular Antioxidants and Green Catalysts. *RSC Adv.* **2020**, *10*, 18583−18593.
(14) Dalla Tiezza, M.; Hamlin, T. A.; Bickelhaupt, F. M.; Orian, L. Radical Scavenging Potential of the Phenothiazine Scaffold A Computational Analysis. *ChemMedChem* **2021**, *16*, 3763−3771.
(15) Shaaban, S.; Vervandier-Fasseur, D.; Andreoletti, P.; Zarrouk, A.; Richard, P.; Negm, A.; Manolikakes, G.; Jacob, C.; Cherkaoui-Malki, M. Cytoprotective and Antioxidant Properties of Organic Selenides for the Myelin-Forming Cells, Oligodendrocytes. *Bioorg. Chem.* **2018**, *80*, 43−56.
(16) Wenthur, C. J.; Bennett, M. R.; Lindsley, C. W. Classics in Chemical Neuroscience: Fluoxetine (Prozac). *ACS Chem. Neurosci.* **2014**, *5*, 14−23.
(17) Daina, A.; Michielin, O.; Zoete, V. SwissADME: A Free Web Tool to Evaluate Pharmacokinetics, Drug-Likeness and Medicinal Chemistry Friendliness of Small Molecules. *Sci. Rep.* **2017**, *7*, No. 42717.
(18) Abid, M.; Azam, A. Synthesis and Antiamoebic Activities of 1-N-Substituted Cyclised Pyrazoline Analogues of Thiosemicarbazones. *Bioorg. Med. Chem.* **2005**, *13*, 2213−2220.
(19) Perrine, D. M.; Sabanayagam, N. R.; Reynolds, K. J. Synthesis of NMP, a Fluoxetine (Prozac) Precursor, in the Introductory Organic Laboratory. *J. Chem. Educ.* **1998**, *75*, 1266.
(20) Wenzel, N. I.; Chavain, N.; Wang, Y.; Friebolin, W.; Maes, L.; Pradines, B.; Lanzer, M.; Yardley, V.; Brun, R.; Herold-Mende, C.; Biot, C.; Tóth, K.; Davioud-Charvet, E. Antimalarial versus Cytotoxic Properties of Dual Drugs Derived From 4-Aminoquinolines and Mannich Bases: Interaction with DNA. *J. Med. Chem.* **2010**, *53*, 3214−3226.
(21) Liou, J.-C.; Badsara, S. S.; Huang, Y.-T.; Lee, C.-F. Syntheses of Selenoesters through C−H Selenation of Aldehydes with Diselenides under Metal-Free and Solvent-Free Conditions. *RSC Adv.* **2014**, *4*, 41237−41244.
(22) Orian, L.; Flohé, L. Selenium-Catalyzed Reduction of Hydroperoxides in Chemistry and Biology. *Antioxidants* **2021**, *10*, 1560.
(23) Arnér, E. S. J.; Holmgren, A. Physiological Functions of Thioredoxin and Thioredoxin Reductase: Thioredoxin and Thioredoxin Reductase. *Eur. J. Biochem.* **2000**, *267*, 6102−6109.
(24) Wolters, L. P.; Orian, L. Peroxidase Activity of Organic Selenides: Mechanistic Insights from Quantum Chemistry. *Curr. Org. Chem.* **2015**, *20*, 189−197.
(25) Tiezza, M. D.; Ribaudo, G.; Orian, L. Organodiselenides: Organic Catalysis and Drug Design Learning from Glutathione Peroxidase. *Curr. Org. Chem.* **2019**, *23*, 1381−1402.
(26) Singh, F. V.; Wirth, T. Selenium Reagents as Catalysts. *Catal. Sci. Technol.* **2019**, *9*, 1073−1091.
(27) Back, T. G. Oxidations Catalyzed By Seleninic Acids and Anhydrides, Their Precursors and Congeners. *Curr. Green Chem.* **2016**, *3*, 76−91.
(28) Santoro, S.; Azeredo, J. B.; Nascimento, V.; Sancineto, L.; Braga, A. L.; Santi, C. The Green Side of the Moon: Ecofriendly Aspects of Organoselenium Chemistry. *RSC Adv.* **2014**, *4*, 31521−31535.
(29) Nogueira, C. W.; Zeni, G.; Rocha, J. B. T. Organoselenium and Organotellurium Compounds: Toxicology and Pharmacology. *Chem. Rev.* **2004**, *104*, 6255−6286.
(30) Arai, K.; Matsunaga, T.; Ueno, H.; Akahoshi, N.; Sato, Y.; Chakrabarty, G.; Mugesh, G.; Iwaoka, M. Modeling Thioredoxin Reductase-Like Activity with Cyclic Selenenyl Sulfides: Participation of an NH···Se Hydrogen Bond through Stabilization of the Mixed Se−S Intermediate. *Chem.−Eur. J.* **2019**, *25*, 12751−12760.
(31) Thurow, S.; Abenante, L.; Anghinoni, J. M.; Lenardão, E. J. Selenium as a Versatile Reagent in Organic Synthesis: More than Allylic Oxidation. *Curr. Org. Synth.* **2021**, *18*, DOI: 10.2174/1570179418666210525152001.
(32) Andersen, J.; Stuhr-Hansen, N.; Zachariassen, L. G.; Koldsø, H.; Schiøtt, B.; Strømgaard, K.; Kristensen, A. S. Molecular Basis for Selective Serotonin Reuptake Inhibition by the Antidepressant Agent Fluoxetine (Prozac). *Mol. Pharmacol.* **2014**, *85*, 703−714.
(33) Wong, D. T.; Perry, K. W.; Bymaster, F. P. The Discovery of Fluoxetine Hydrochloride (Prozac). *Nat. Rev. Drug. Discov.* **2005**, *4*, 764−774.
(34) Staroń, J.; Pietruś, W.; Bugno, R.; Kurczab, R.; Satała, G.; Warszycki, D.; Lenda, T.; Wantuch, A.; Hogendorf, A. S.; Hogendorf, A.; Duszyńska, B.; Bojarski, A. J. Tuning the Activity of Known Drugs via the Introduction of Halogen Atoms, a Case Study of SERT Ligands − Fluoxetine and Fluvoxamine. *Eur. J. Med. Chem.* **2021**, *220*, No. 113533.
(35) Mohanty, S.; Reddy, S. G.; RamaDevi, B.; Karmakar, A. C. An Assembly of Structurally Diverse Small and Simple 5-Aminomethylene Derivatives of 2,4-Thiazolidinedione and Studies of Their Biological Activity. *Med. Chem. Res.* **2015**, *24*, 4037−4049.
(36) Galano, A.; Alvarez-Idaboy, J. R. A Computational Methodology for Accurate Predictions of Rate Constants in Solution: Application to the Assessment of Primary Antioxidant Activity. *J. Comput. Chem.* **2013**, *34*, 2430−2445.
(37) Bortoli, M.; Dalla Tiezza, M.; Muraro, C.; Pavan, C.; Ribaudo, G.; Rodighiero, A.; Tubaro, C.; Zagotto, G.; Orian, L. Psychiatric Disorders and Oxidative Injury: Antioxidant Effects of Zolpidem Therapy Disclosed In Silico. *Comput. Struct. Biotechnol. J.* **2019**, *17*, 311−318.
(38) Wood, K. M.; Zeqja, A.; Nijhout, H. F.; Reed, M. C.; Best, J.; Hashemi, P. Voltammetric and Mathematical Evidence for Dual

https://doi.org/10.1021/acsomega.1c05567
ACS Omega 2022, 7, 8314−8322

Transport Mediation of Serotonin Clearance *in Vivo*. *J. Neurochem.* **2014**, *130*, 351−359.
(39) Hashemi, P.; Dankoski, E. C.; Petrovic, J.; Keithley, R. B.; Wightman, R. M. Voltammetric Detection of 5-Hydroxytryptamine Release in the Rat Brain. *Anal. Chem.* **2009**, *81*, 9462−9471.
(40) West, A.; Best, J.; Abdalla, A.; Nijhout, H. F.; Reed, M.; Hashemi, P. Voltammetric Evidence for Discrete Serotonin Circuits, Linked to Specific Reuptake Domains, in the Mouse Medial Prefrontal Cortex. *Neurochem. Int.* **2019**, *123*, 50−58.
(41) Saylor, R. A.; Hersey, M.; West, A.; Buchanan, A. M.; Berger, S. N.; Nijhout, H. F.; Reed, M. C.; Best, J.; Hashemi, P. In Vivo Hippocampal Serotonin Dynamics in Male and Female Mice: Determining Effects of Acute Escitalopram Using Fast Scan Cyclic Voltammetry. *Front. Neurosci.* **2019**, *13*, No. 362.
(42) Abdalla, A.; West, A.; Jin, Y.; Saylor, R. A.; Qiang, B.; Peña, E.; Linden, D. J.; Nijhout, H. F.; Reed, M. C.; Best, J.; Hashemi, P. Fast Serotonin Voltammetry as a Versatile Tool for Mapping Dynamic Tissue Architecture: I. Responses at Carbon Fibers Describe Local Tissue Physiology. *J. Neurochem.* **2020**, *153*, 33−50.
(43) Jackson, B. P.; Dietz, S. M.; Wightman, R. Mark. Fast-Scan Cyclic Voltammetry of 5-Hydroxytryptamine. *Anal. Chem.* **1995**, *67*, 1115−1120.
(44) Hersey, M.; Samaranayake, S.; Berger, S. N.; Tavakoli, N.; Mena, S.; Nijhout, H. F.; Reed, M. C.; Best, J.; Blakely, R. D.; Reagan, L. P.; Hashemi, P. Inflammation-Induced Histamine Impairs the Capacity of Escitalopram to Increase Hippocampal Extracellular Serotonin. *J. Neurosci.* **2021**, *41*, 6564−6577.
(45) Kreilgaard, M.; Smith, D. G.; Brennum, L. T.; Sánchez, C. Prediction of Clinical Response Based on Pharmacokinetic/Pharmacodynamic Models of 5-Hydroxytryptamine Reuptake Inhibitors in Mice: Clinical Predictions by PK/PD Modelling in Mice. *Br. J. Pharmacol.* **2008**, *155*, 276−284.
(46) Zhao, Y.; Truhlar, D. G. The M06 Suite of Density Functionals for Main Group Thermochemistry, Thermochemical Kinetics, Noncovalent Interactions, Excited States, and Transition Elements: Two New Functionals and Systematic Testing of Four M06-Class Functionals and 12 Other Functionals. *Theor. Chem. Acc.* **2008**, *120*, 215−241.
(47) Frisch, M. J.; Trucks, G. W.; Schlegel, H. B.; Scuseria, G. E.; Robb, M. A.; Cheeseman, J. R.; Scalmani, G.; Barone, V.; Petersson, G. A.; Nakatsuji, H.; Li, X.; Caricato, M.; Marenich, A. V.; Bloino, J.; Janesko, B. G.; Gomperts, R.; Mennucci, B.; Hratchian, H. P.; Ortiz, J. V.; Izmaylov, A. F.; Sonnenberg, J. L.; Williams; Ding, F.; Lipparini, F.; Egidi, F.; Goings, J.; Peng, B.; Petrone, A.; Henderson, T.; Ranasinghe, D.; Zakrzewski, V. G.; Gao, J.; Rega, N.; Zheng, G.; Liang, W.; Hada, M.; Ehara, M.; Toyota, K.; Fukuda, R.; Hasegawa, J.; Ishida, M.; Nakajima, T.; Honda, Y.; Kitao, O.; Nakai, H.; Vreven, T.; Throssell, K.; Montgomery, J. A., Jr.; Peralta, J. E.; Ogliaro, F.; Bearpark, M. J.; Heyd, J. J.; Brothers, E. N.; Kudin, K. N.; Staroverov, V. N.; Keith, T. A.; Kobayashi, R.; Normand, J.; Raghavachari, K.; Rendell, A. P.; Burant, J. C.; Iyengar, S. S.; Tomasi, J.; Cossi, M.; Millam, J. M.; Klene, M.; Adamo, C.; Cammi, R.; Ochterski, J. W.; Martin, R. L.; Morokuma, K.; Farkas, O.; Foresman, J. B.; Fox, D. J. *Gaussian 16*, Rev. C.01; Gaussian Inc.: Wallingford, CT, 2016.
(48) Marenich, A. V.; Cramer, C. J.; Truhlar, D. G. Universal Solvation Model Based on Solute Electron Density and on a Continuum Model of the Solvent Defined by the Bulk Dielectric Constant and Atomic Surface Tensions. *J. Phys. Chem. B* **2009**, *113*, 6378−6396.
(49) Galano, A. On the Direct Scavenging Activity of Melatonin towards Hydroxyl and a Series of Peroxyl Radicals. *Phys. Chem. Chem. Phys.* **2011**, *13*, 7178.
(50) Mena, S.; Dietsch, S.; Berger, S. N.; Witt, C. E.; Hashemi, P. Novel, User-Friendly Experimental and Analysis Strategies for Fast Voltammetry: 1. The Analysis Kid for FSCV. *ACS Meas. Sci. Au* **2021**, *1*, 11−19.
(51) Charan, J.; Kantharia, N. How to Calculate Sample Size in Animal Studies? *J. Pharmacol. Pharmacother.* **2013**, *4*, 303−306.
(52) Cohen, J. *Statistical Power Analysis for the Behavioral Sciences*, 2nd ed. Routledge: New York, 1988.

https://doi.org/10.1021/acsomega.1c05567
ACS Omega 2022, 7, 8314−8322